Water Transport Properties of the Grape Pedicel during Fruit Development: Insights into Xylem Anatomy and Function Using Microtomography[1][OPEN]

Thorsten Knipfer*, Jiong Fei, Gregory A. Gambetta[2], Andrew J. McElrone, Kenneth A. Shackel, and Mark A. Matthews*

Department of Viticulture and Enology (T.K., J.F., G.A.G., A.J.M., M.A.M.) and Department of Plant Sciences/Pomology (K.A.S.), University of California, Davis, California 95616; and United States Department of Agriculture-Agricultural Research Service, Crops Pathology and Genetics Research Unit, Davis, California 95616 (A.J.M.)

ORCID IDs: 0000-0001-5945-7273 (T.K.); 0000-0002-8838-5050 (G.A.G.).

Xylem flow of water into fruits declines during fruit development, and the literature indicates a corresponding increase in hydraulic resistance in the pedicel. However, it is unknown how pedicel hydraulics change developmentally in relation to xylem anatomy and function. In this study on grape (*Vitis vinifera*), we determined pedicel hydraulic conductivity (k_h) from pressure-flow relationships using hydrostatic and osmotic forces and investigated xylem anatomy and function using fluorescent light microscopy and x-ray computed microtomography. Hydrostatic k_h (xylem pathway) was consistently 4 orders of magnitude greater than osmotic k_h (intracellular pathway), but both declined before veraison by approximately 40% and substantially over fruit development. Hydrostatic k_h declined most gradually for low (less than 0.08 MPa) pressures and for water inflow and outflow conditions. Specific k_h (per xylem area) decreased in a similar fashion to k_h despite substantial increases in xylem area. X-ray computed microtomography images provided direct evidence that losses in pedicel k_h were associated with blockages in vessel elements, whereas air embolisms were negligible. However, vessel elements were interconnected and some remained continuous postveraison, suggesting that across the grape pedicel, a xylem pathway of reduced k_h remains functional late into berry ripening.

In grape (*Vitis vinifera*), fruit growth by water accumulation follows a double sigmoid pattern and is influenced by the diurnal and developmental changes in water flow between fruit and the parent plant (Matthews and Shackel, 2005). Until the onset of fruit ripening (i.e. veraison), water enters the fruit predominantly via the xylem and thereafter mainly through the phloem (Greenspan et al., 1994, 1996). Choat et al. (2009) showed that the hydraulic conductance (i.e. 1/resistance) of the grape berry and pedicel declines substantially at later ripening stages predominantly due to a decline in pedicel conductance. Significant developmental changes in pedicel hydraulic properties were also reported for tomato (*Solanum lycopersicum*) and were found to be associated with xylem anatomical changes (Lee 1989; Van Ieperen et al., 2003; Rancić et al., 2008, 2010). Due to its position along the vascular transport pathway between fruit and the parent plant, the pedicel can play an important role in affecting fruit growth, as in kiwi (*Actinidia deliciosa*; Mazzeo et al., 2013). However, for grape, it needs to be elucidated how pedicel hydraulic properties change developmentally in relation to xylem anatomy and function.

The location and nature of the loss in hydraulic conductance between the parent plant and the fruit is unclear and may differ among fruits. For tomato, Malone and Andrews (2001) showed that most of the loss of hydraulic conductance occurs in the fruit per se, but Van Ieperen et al. (2003) reported important and decreasing hydraulic conductance in the pedicel abscission zone over fruit development. For *Citrus* spp., Garcia-Luis et al. (2002) reported that xylem vessels in the pedicel remain largely functional late into fruit ripening. For grape, although vessel breakage in the berry was thought to lead to xylem dysfunction (Coombe and McCarthy 2000),

[1] This work was supported by the U.S. Department of Agriculture/Cooperative State Research, Education, and Extension Service (grant no. 2006–35100–17440). The Advanced Light Source is supported by the Director, Office of Science, Office of Basic Energy Sciences, U.S. Department of Energy (contract no. DE–AC02–05CH11231).

[2] Present address: Institute des Sciences de la Vigne et du Vin, 51bis Rue Alfred Charlionnet, 33400 Talence, Bordeaux, France.

* Address correspondence to knipfer.thorsten@yahoo.de and mamatthews@ucdavis.edu.

The author responsible for distribution of materials integral to the findings presented in this article in accordance with the policy described in the Instructions for Authors (www.plantphysiol.org) is: Thorsten Knipfer (knipfer.thorsten@yahoo.de).

T.K. performed all the experiments, analyzed the data, and wrote the article; J.F. and G.A.G. helped in sample preparation for microscopy and experimental design and revised the article; A.J.M. helped in sample preparation for x-ray computed tomography and revised the article; K.A.S. contributed to the data analysis and revised the article; M.A.M. acted as the supervisor, obtained the grants related to the work, and helped to prepare and revise the article.

[OPEN] Articles can be viewed without a subscription.

www.plantphysiol.org/cgi/doi/10.1104/pp.15.00031

several studies and methods have shown that xylem vessels in the fruit remain functional (Rogiers et al., 2001; Bondada et al., 2005; Chatelet et al., 2008a, 2008b). In line with these findings, data by Keller et al. (2006) suggest that the pedicel xylem also remains at least partially functional in ripening grape berries and can conduct water to and from the parent plant. Nevertheless, a reduction in the ability to transport water during ripening has been reported for grape (Tyerman et al., 2004; Choat et al., 2009) and other fleshy fruits, such as apple (*Malus domestica*; Lang and Ryan, 1994) and kiwi (Mazzeo et al., 2013), and it still remains unclear what causes this loss in xylem hydraulic conductance. For the grape pedicel, Choat et al. (2009) detected higher concentrations of xylem solutes postveraison and proposed that this is related to the deposition of gels into the xylem vessel lumen. However, direct evidence for the presence of xylem blockage and/or embolism formation in the grape pedicel is missing.

This study of the grape 'Cabernet Sauvignon' pedicel was conducted with the goal to obtain a comprehensive understanding of how changes in hydraulic properties relate to changes in xylem structure and function over fruit development. Over the course of fruit development from 20 to 90 d after anthesis (DAA), water transport properties of pedicels were investigated under osmotic and hydrostatic driving forces using a modified pressure-probe system. This was combined with analyses of spatial and temporal changes in pedicel xylem anatomy and function using fluorescent light microscopy and x-ray computed microtomography (microCT; Brodersen et al., 2010, 2013; Rancić et al., 2010).

RESULTS

Fruit and Pedicel Enlargement

From 20 to 90 DAA, fruit enlargement was evident from an increase in fruit diameter and followed three stages (I, less than 40 DAA; II, 40–55 DAA; and III, more than 55 DAA; Fig. 1A). The transition from stage II to stage III coincided with veraison. Fruit solute potential started to decrease before veraison during stage II from an average of −0.82 to −1.54 MPa and continued to decrease in stage III to an average of −3.97 MPa (Fig. 1A). Enlargement of the pedicel receptacle and stem portion ceased before and around veraison, respectively (Fig. 1, B and C). Pedicel receptacle diameters increased mainly in stage I from an average of 2.9 to 3.4 mm but changed little thereafter (Fig. 1B). Pedicel stem diameters increased until the end of stage II from an average of 1.3 to 1.7 mm (Fig. 1C). Pedicel length remained at approximately 4 mm throughout fruit development (Fig. 1D).

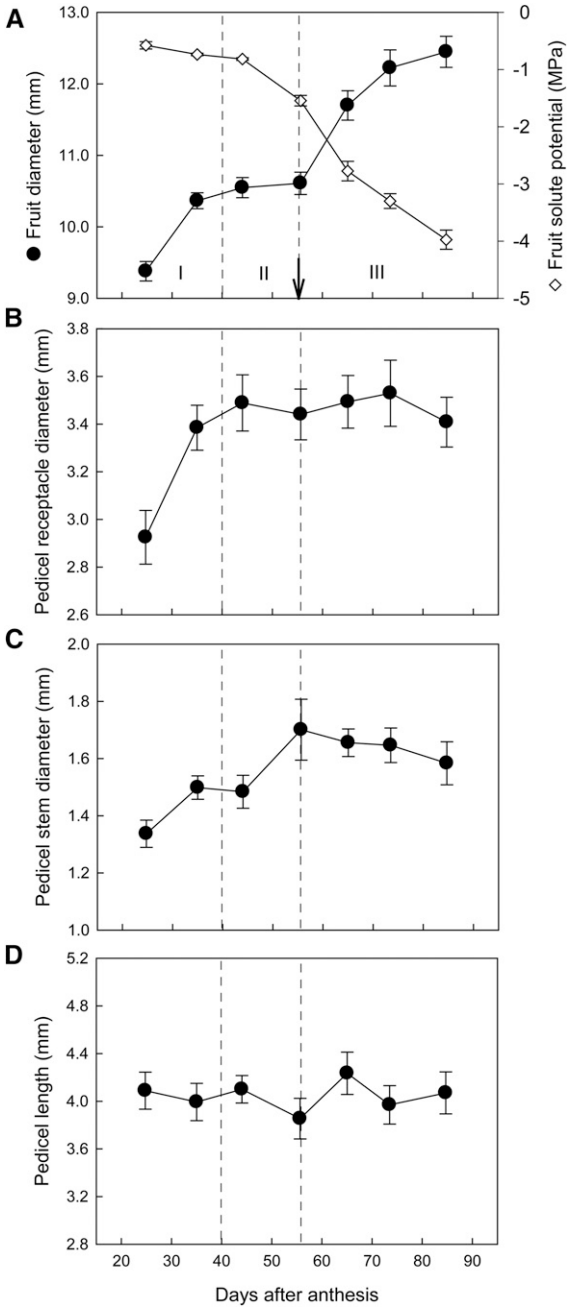

Figure 1. Developmental changes in fruit diameter and solute potential (A), pedicel diameter of receptacle portion (B), pedicel diameter of stem portion (C), and pedicel length (D). The dashed lines indicate the estimated boundaries between stages I and II and stages II and III in fruit expansion, and the arrow indicates veraison (i.e. 50% change in skin color). Data are means ± SE (n = 7–31).

Spatial and Temporal Arrangement of Xylem

Transverse light microscopy images of the pedicel stem and receptacle portion show that the vascular system consisted of heavily lignified xylem tissue that was separated by less lignified ray cells (Fig. 2). The enlarged image of the stem portion highlights that phloem tissue was located in close proximity to the outer peripheral xylem tissue and was bordered by lignified fiber cap cells in the cortex (Fig. 2A). Fiber cap cells were most pronounced in the pedicel stem portion. Over fruit development, in pedicel stem (Fig. 2B, row 1) and receptacle

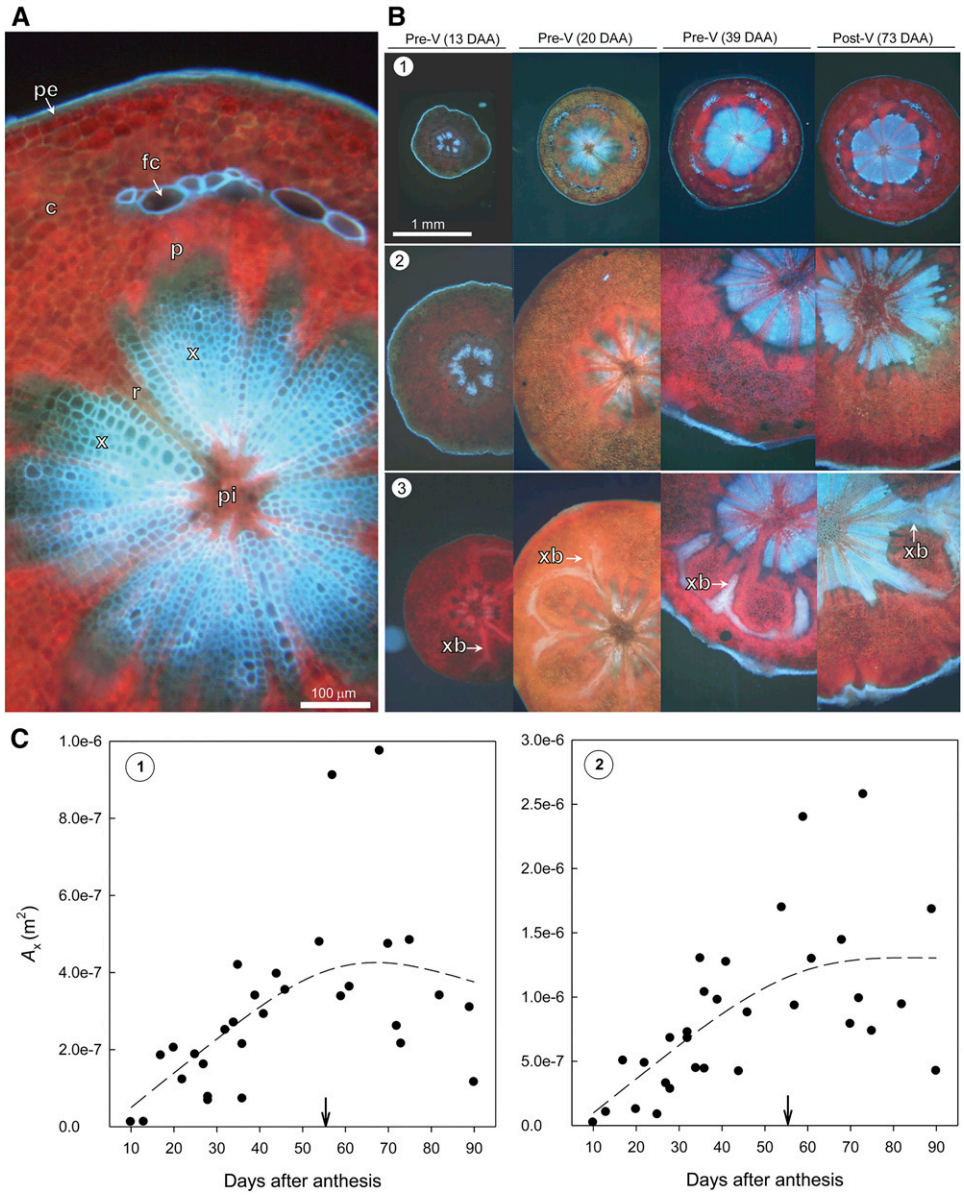

Figure 2. Free-hand cross sections of pedicels imaged unstained under violet fluorescent light over fruit development. Lignified tissue appears in bright blue color. A, Enlarged image of the pedicel stem portion indicating the presence of various tissue types. c, Cortex; fc, fiber cap cells; p, phloem; pe, periderm, pi, pith; r, less lignified ray cells; x, lignified xylem tissue. B, Spatial and temporal changes in pedicel dimensions and xylem cross-sectional area of stem portion (see row 1, position 1 in Fig. 10) and receptacle portion (see rows 2 and 3, positions 2 and 3 in Fig. 10, respectively). In the receptacle portion close to the fruit, radial branches of xylem tissue (xb) into the cortex are visible (row 3), which increase in intensity over fruit development. V, Veraison. C, Developmental changes in A_x in stem portion (image 1, left) and receptacle portion (image 2, right). Dashed lines indicate 75% smoothed trend lines. The arrows indicate veraison.

portion (Fig. 2B, rows 2 and 3), cross-sectional areas of heavily lignified xylem tissue (A_x) increased mainly up to veraison (Fig. 2C). From 20 to 90 DAA, A_x in the pedicel stem portion increased by approximately 2.7-fold and in the receptacle portion by approximately 4-fold. Comparing both pedicel portions, A_x of the stem portion was more than 2-fold smaller than the receptacle portion. A unique feature of the receptacle portion in proximity to the fruit was radial branches of lignified xylem tissue stretching into the cortex (Fig. 2B, row 3), which potentially connect with peripheral vascular bundles in the fruit.

Hydraulic Properties

For pedicels analyzed between 20 and 90 DAA, hydraulic conductivity (k_h) was derived from pressure-flow relationships as measured under hydrostatically and osmotically driven water flows (Fig. 3). The rate of volume flow (Q) induced hydrostatically ramped up when the hydrostatic pressure gradient (ΔP) exceeded 0.08 MPa (Fig. 3A), and the pressure-flow relationship was typically composed of two linear parts of $\Delta P = -0.05$ to 0.08 MPa and $\Delta P > 0.08$ MPa (for pressure-flow characteristics of two additional pedicels, see Supplemental Figs. S1 and S2). In osmotic experiments, Q was much smaller than in hydrostatic experiments, and for the osmotic pressure gradient ($\Delta\pi$) of 0.6 to 3.1 MPa, the pressure-flow relationship was assumed to be linear (Fig. 3B). Pedicel k_h under osmotically and hydrostatically driven water flows were derived from the slopes of the corresponding linear regression lines.

Pedicel hydrostatic and osmotic k_h declined by approximately 40% until veraison (55 DAA) and

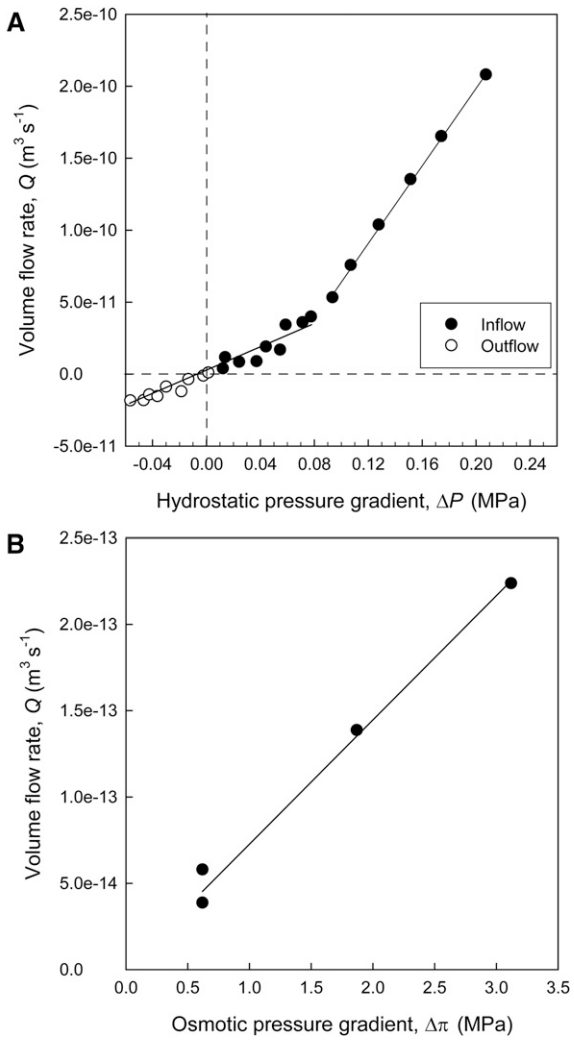

Figure 3. Representative pressure-flow relationships of an excised pedicel as measured with a modified pressure-probe system (Supplemental Figs. S1 and S2). A volume flow of water was induced across the pedicel by the application of hydrostatic (A) or osmotic (B) pressure forces. Solid lines are linear regression lines fitted to linear parts of the pressure-flow relationship (i.e. low $\Delta P = -0.05$ to 0.08 MPa [$r^2 = 0.90$], high ΔP is greater than 0.08 MPa [$r^2 = 0.99$], and $\Delta\pi =$ 0.6 to 3.3 MPa [$r^2 = 0.93$]).

substantially over fruit development (Fig. 4). Hydrostatic k_h as measured from multiple and low ΔP values (0.08 MPa or less) declined gradually and significantly by approximately 3-fold from 32 DAA (stage I) to 62 DAA (early stage III; Fig. 4A). In comparison, hydrostatic k_h as measured from high ΔP values (greater than 0.08 MPa) was typically 2-fold greater, and corresponding losses in pedicel k_h were less gradual (Fig. 4A). Similar to hydrostatic k_h, osmotic k_h declined significantly by approximately 2-fold from 30 DAA to 76 DAA but was consistently 3 to 4 orders of magnitude lower than hydrostatic k_h (Fig. 4A). Based on measurements using low ΔP values, pedicel hydrostatic k_h was also determined exclusively for water inflow (i.e. 0–0.08 MPa) and outflow (i.e. −0.05 to 0 MPa) conditions (Fig. 4B). Hydrostatic k_h values for both directions of water flow were comparable, but under water outflow conditions, early development changes in k_h were most pronounced. When hydrostatic k_h as measured from low ΔP values was normalized for A_x of pedicel stem or receptacle portion (Fig. 4C), k_s declined significantly from 32 DAA (stage I) to 62 DAA (early stage III) for both pedicel portions, which was similar to the developmental reduction in k_h.

Xylem Structure and Function

Transverse microCT images of representative pedicels show that xylem tissue was water filled both preveraison and postveraison (Fig. 5, A–C). Air-filled tissue was only detected in the pith of pedicel receptacle (Fig. 5, A and B) and stem (Fig. 5C) portion; if any, a few xylem vessel elements ($n < 5$) were air filled close to the pith. For comparison, the microCT image of a dehydrated pedicel shows the large number of air-filled elements (n = 1,700; Supplemental Fig. S3) in the pedicel stem xylem portion (Fig. 5D).

The lumen of vessel elements in the pedicel stem portion became interrupted mainly postveraison (Fig. 6). Representative 3-D images show volume renderings of the pedicel surface (Fig. 6, A–C) and vessel elements extracted from this portion (Fig. 6, D–F), and longitudinal two-dimensional (2-D) images show vessel elements embedded in the pedicel tissue (Fig. 6, G–I). Early in fruit development, at 20 and 40 DAA, vessel lumen was mainly continuous (vessel elements A–E, G–J, and L) and rarely constricted (vessel element F) or interrupted (vessel element K). After veraison at 80 DAA, the lumen of many vessel elements was interrupted at multiple positions along vessel elements (vessel elements M–O and R); interruptions were 2 to 12 μm in length. A quantitative analysis predicted that, postveraison, an average of 46% of vessel elements in the pedicel stem portion were interrupted by blockages, whereas only 6% of vessel elements were interrupted before veraison ($P < 0.01$; Table I).

Higher resolution 3-D images generated from a postveraison pedicel at 85 DAA (Fig. 7) revealed that, at positions where vessel elements were constricted (vessel element A at positions 1 and 2 and vessel element C at position 4) or interrupted (vessel element B at position 3 and vessel element D at position 5), solid material emerged into the vessel lumen and ultimately blocked the interior.

The structure and spatial arrangement of vessel elements in the pedicel stem portion was rather complex (Fig. 8). Vessel elements of variable length (range from 204–530 μm, diameter of 5–15 μm; in tomato, length = 60–560 μm, diameter = 8–53 μm; Rancić et al., 2008, 2010) were packed very closely (Fig. 8A). Vessel elements had a tracheid-like shape with oblique end walls and diameters of vessel elements varied along their length (Fig. 8B). Vessel elements were not aligned

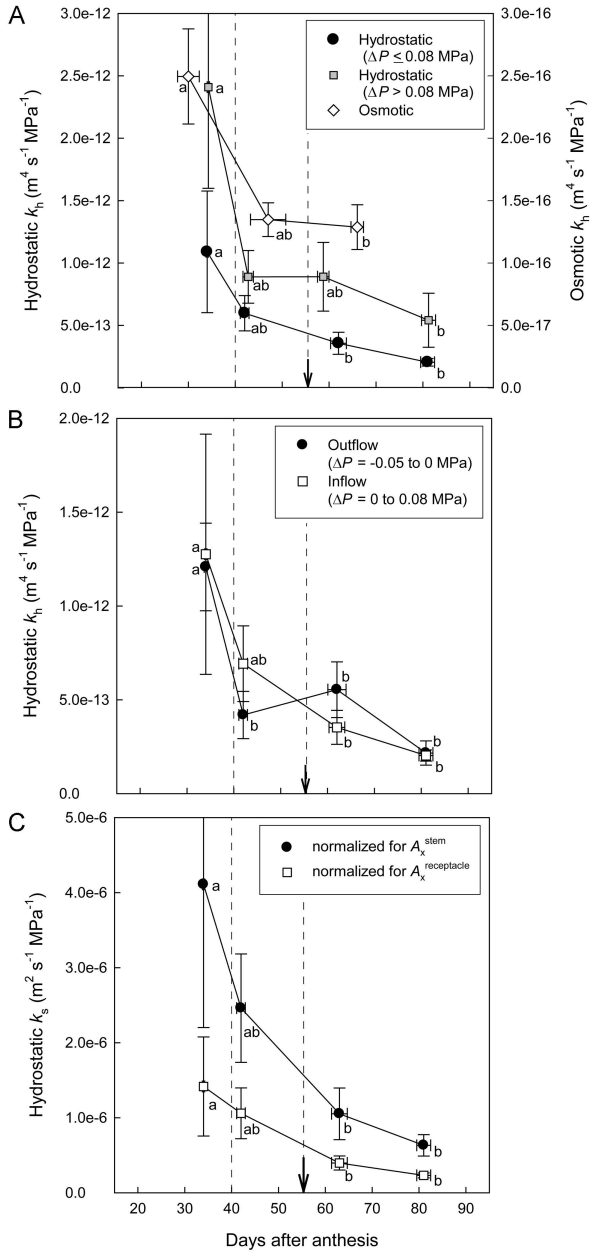

Figure 4. Developmental changes in pedicel hydraulic properties as measured directly on excised pedicels using a modified pressure-probe system. A, Pedicel k_h was determined for hydrostatically and osmotically induced water flows (note the difference in *y* scales). Based on the pressure-flow characteristics of the pedicel, hydrostatic k_h was derived separately from low-ΔP (−0.05 to 0.08 MPa) and high-ΔP (greater than 0.08 MPa) steps. B, Pedicel hydrostatic k_h as determined under water inflow and outflow conditions using low ΔP values. C, Specific hydraulic conductivity (k_s) as determined by normalizing hydrostatic k_h measured under low ΔP for A_x of either stem or receptacle portion. Data are means ± SE. In A, n = 4, 5, 13, and 5 (black circles), n = 4, 4, 8, and 5 (gray squares), and n = 5, 3, and 9 (white diamonds); in B, n = 4, 5, 13, and 5 (white squares) and n = 3, 5, 6, 4 (black circles); in C, n = 4, 5, 13, and 5 for samples analyzed at less than 40 DAA (stage I), 40 to 55 DAA (stage II), 55 to 75 DAA (stage III), and 75 to 90 DAA (stage III), respectively. When SE is smaller than the symbol size, it is not visible. For each parameter, different letters indicate significant differences ($P < 0.05$) between means (Tukey-Kramer test). The arrows indicate veraison. Dashed lines indicate the estimated boundaries between stages I and II and stages II and III in fruit expansion (Fig. 1A).

vertically, and continuous vessels through the pedicel were not detected. Using the maceration technique highlighted that vessel elements were of the scalariform type having simple perforation plates (Fig. 8C). Because blockages within the lumen of vessel elements were aligned horizontally and were not in proximity to end walls (Fig. 8B), vessel blockages detected in microCT images were not associated with the presence of perforation plates (Fig. 8C).

Vessel elements in the pedicel stem portion were interconnected postveraison (Fig. 9; same pedicel as shown in Fig. 8). Intervessel connections were detected all along vessel elements A to E with n = 15 to 34 connections per vessel element (Fig. 9B). In theory, intervessel connections facilitate the axial flow of water across the pedicel between vessel elements and in the presence of vessel elements with blockages.

DISCUSSION

For grape, our data show that pedicel k_h under both hydrostatically and osmotically driven water flow starts to decline before veraison and is reduced substantially in early ripening stages (approximately 65 DAA). Gradual changes in pedicel hydrostatic k_h from 30 to 90 DAA were most pronounced when measured from multiple and low ΔP steps. Previous studies only reported significant changes in pedicel hydraulic properties for later stages of ripening (Tyerman et al., 2004; Choat et al., 2009; more than 80 DAA), when most water transport to the berry is already via the phloem (Greenspan et al., 1994). The losses in pedicel k_h over fruit development, as found here, occurred despite 3- and 4-fold increases in xylem cross-sectional area of pedicel stem and receptacle portion, respectively, pointing to important changes in xylem function. The microCT images provided direct evidence that decreasing pedicel k_h was associated with the formation of blockages in the lumen of water-conducting vessel elements (i.e. occlusions, as proposed by Choat et al. [2009]) and not air embolism formation. A quantitative analysis showed that postveraison xylem blockages were present in approximately 50% of all vessel elements. However, vessel elements in the pedicel were interconnected postveraison, suggesting that a functional xylem flow path still exists late into berry ripening.

The diameters of the pedicel receptacle and stem portion increased until 42 and 55 DAA, respectively. These increases were accompanied by developmental increases in xylem cross-sectional area in both pedicel portions. Due to the fact that pedicel k_h was greatest in stage I (less than 40 DAA), when A_x was the smallest, losses of pedicel k_h during development cannot be attributed to xylem area-related limitations of water transport, as reported for tomato (Lee, 1989); this is also evident from the decline in

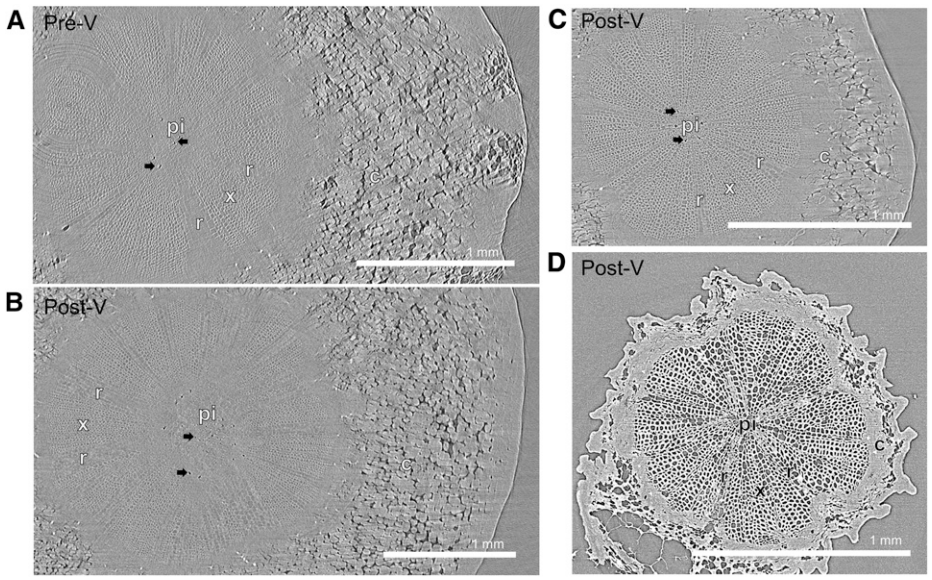

Figure 5. Representative transverse microCT images through the pedicel showing water-filled tissue in light gray and air-filled tissue in dark gray. Black arrows indicate some air-filled tissue in the pith. A and B, Receptacle portion (i.e. position 2 in Fig. 10) of pedicels scanned preveraison at 34 DAA (A) and postveraison at 76 DAA (B). C, Stem portion scanned at 76 DAA (i.e. position 1 in Fig. 10). These images were acquired from pedicels that were scanned immediately after they were cut under water from fruit and rachis. D, Stem portion of a dehydrated pedicel scanned at 85 DAA. c, Cortex; pi, pith; r, ray cells; x, xylem tissue.

pedicel k_s (i.e. k_h per A_x) over fruit development. The negligible effect of developmental changes in xylem area dimensions on pedicel hydraulic properties is evident when comparing hydraulic characteristics of pedicel receptacle versus stem portion: even though A_x of the receptacle is approximately 2-fold greater than that of the stem portion, the limiting hydraulic conductance along the pedicel is located in the receptacle (Choat et al., 2009; see our k_s estimates). For apple, developmental increases in pedicel xylem area are largely due to the proliferation of nonconducting xylem elements (Lang and Ryan, 1994; Horbens et al., 2014), and this may also be the case for grape in order to support higher fruit weight during ripening.

The data presented here revealed that pedicel k_h in grape declines before veraison (i.e. by approximately

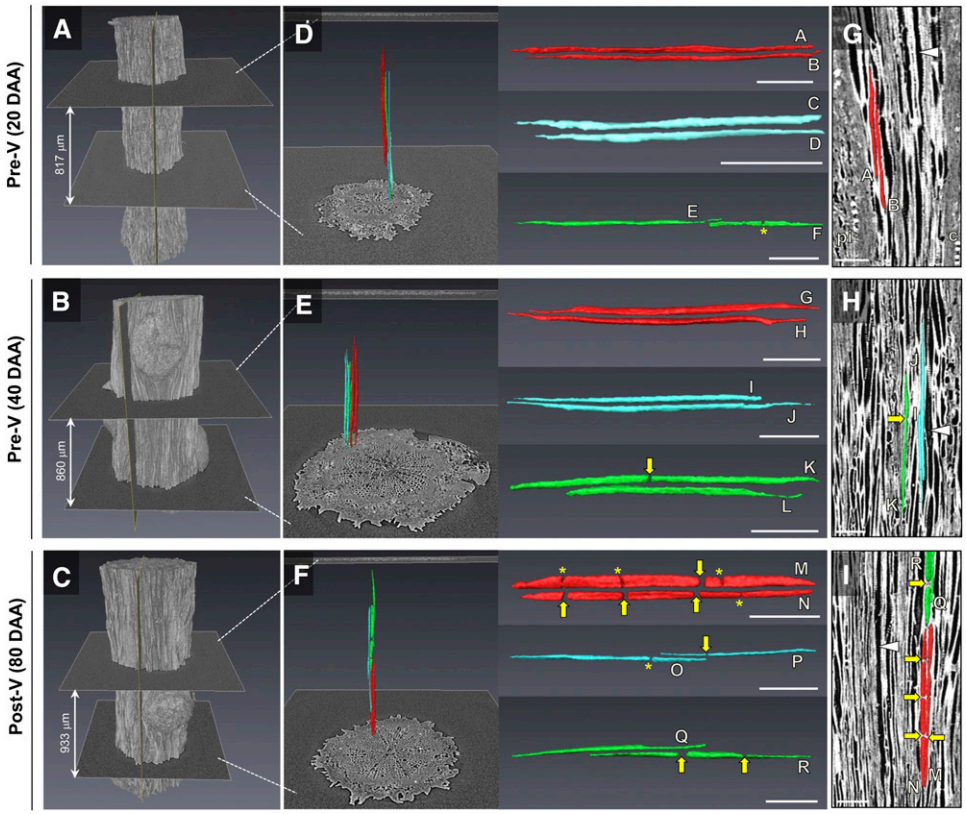

Figure 6. Three-dimensional (3-D) reconstructions of xylem vessel elements in the pedicel stem portion at 20, 40, and 80 DAA. Pedicels were scanned after dehydration. A to C, Volume renderings of the pedicel surface. D to F, Reconstructed vessel elements (n = 6 each) within that pedicel portion. Images to the right show enlarged versions of these reconstructed vessel elements. For better visualization, pairs of vessel elements that were located in close proximity to each other are given the same color (i.e. red, turquoise, or green). G to I, 2-D images of reconstructed vessel elements as they are embedded in the pedicel apoplast (light gray; air-filled vessel lumen is shown in dark gray, as indicated by white arrowheads). The positions of the longitudinal 2-D image slices are indicated in A to C. c, Cortex; pi, pith. Asterisks indicate constricted vessel lumen. Yellow arrows indicate positions where the continuity of the vessel lumen is interrupted. Bars = 100 μm.

Table I. *Quantification of the frequency of vessel elements with blockages (i.e. occlusions) in the grape pedicel stem portion from microCT images*

For each pedicel, vessel elements that intersected the same transverse image slice were generated in 3-D projection and evaluated along their axial distance for the presences of blockages. Different letters indicate significant differences ($P < 0.01$) between means (Student's *t* test).

Developmental Stage	Sample	Total No. of Vessel Elements Analyzed	No. of Vessel Elements with Blockages	Percentage of Vessel Elements with Blockages
Preveraison	1 (20 DAA; Fig. 6)	47	2	4
	2 (40 DAA; Fig. 6)	46	3	7
	3 (35–45 DAA)	49	4	8
				6.3 ± 2 (mean ± SD) a
Postveraison	4 (80 DAA; Fig. 6)	59	28	47
	5 (85 DAA; Figs. 7–9)	49	22	45
	6 (90–100 DAA)	46	21	46
				46 ± 1.3 (mean ± SD) b

40%) and substantially in early stages of berry ripening. This was the case when measured osmotically and hydrostatically, under both low (−0.05 to 0.08 MPa) and high (greater than 0.08 MPa) ΔP. Due to the fact that pedicel length did not change developmentally, it can be predicted that, in the intact plant, pedicel osmotic and hydrostatic hydraulic conductance (in $m^3\ s^{-1}\ MPa^{-1}$) changes in a similar fashion. However, the reduction in hydrostatic pedicel k_h from stage I to stage III was most gradual when measured under low ΔP. Because water flow through the pedicel ramped up for ΔP greater than 0.08 MPa, our data suggest that, under high ΔP, water flow is induced not exclusively through xylem vessel elements but also through the apoplastic space. Similar findings were reported by Van Ieperen et al. (2003) for tomato and Mazzeo et al. (2013) for kiwi. This would explain why pedicel hydrostatic k_h obtained from high ΔP was always greater than the one from low ΔP. Choat et al. (2009) analyzed grape 'Chardonnay' pedicel hydraulics from a single and high ΔP of 0.1 MPa without having knowledge about the pressure-flow relationship and found that hydraulic properties change only in later stages of berry ripening. In comparison with our study on grape 'Cabernet Sauvignon,' this may indicate that grape pedicels from different grape varieties differ in their developmental changes in hydraulic properties. On the other hand, pedicel hydraulics measured from a single and high ΔP most likely lack the accuracy necessary to resolve the early developmental changes in k_h. Hence, it is recommended that developmental changes in grape pedicel hydraulics should be measured from pressure-flow relationships established using multiple ΔP values, and low (less than 0.08 MPa) ΔP steps should be used to minimize apoplastic bypass flows that may potentially mask real developmental changes in xylem hydraulic properties.

Water flow across the pedicel is driven by a gradient in water potential between the parent plant and berry. Developmental changes in berry skin transpiration and sugar accumulation impact the hydrostatic and osmotic pressure components, respectively, of berry water potential (Matthews and Shackel, 2005). However, gradients in hydrostatic and osmotic pressure can induce water flow along different pathways (Steudle, 2000). In theory, hydrostatically driven water flow follows predominantly an extracellular low-resistance pathway, whereas osmotically driven water flow follows mainly a high-resistance pathway that involves crossing of osmotic barriers (e.g. cell membranes and apoplastic barriers). In order to obtain a complete picture of pedicel hydraulic properties, pedicel k_h was determined under both driving forces. Based on the composite transport model of water flow, it can be concluded that pedicel k_h obtained from low ΔP (−0.05 to 0.08 MPa) represents mainly the hydraulic property of a hydraulic pathway along xylem vessel elements, whereas high ΔP (greater than 0.08) induces an additional apoplastic bypass flow through the cell wall space. A predominant water flow driven osmotically requires the presence of osmotic barrier(s) that prevent the free diffusion of solutes. In this study, depositions of osmotic barriers in the pedicel apoplast, such as Casparian band-like structures, were not detected (data not shown); the apoplastic space between vessel elements is in biophysical terms an inefficient osmotic barrier; therefore, osmotically driven flow, if any, is relatively small. Hence, pedicel osmotic k_h represents mainly the hydraulic property of a high-resistance membrane-bound pathway through cortex, pith, and phloem tissue, excluding a predominant flow through vessel elements. The loss in pedicel osmotic k_h over fruit development may be associated with a decline in aquaporin activity in the pedicel, as has been found for some aquaporin isoforms in the berry (Fouquet et al., 2008; Choat et al., 2009). Moreover, a membrane-bound transport pathway through the pedicel may also be affected developmentally by structural changes of cells (Nii and Coombe, 1983). Based on findings that cells in healthy berries and rachis remain largely viable postveraison (Krasnow et al., 2008; Hall et al., 2011), it can be speculated that a membrane-bound pathway through the pedicel of reduced k_h most likely exists late into fruit ripening. However, since pedicel osmotic k_h was 3 to 4 orders of magnitude smaller than hydrostatic k_h, membrane-bound water flows through the pedicel may only contribute substantially to overall fruit water uptake when water enters the fruit predominantly via the phloem or when xylem flows, if present, are primarily in the reverse direction (i.e. postveraison; Greenspan et al., 1994).

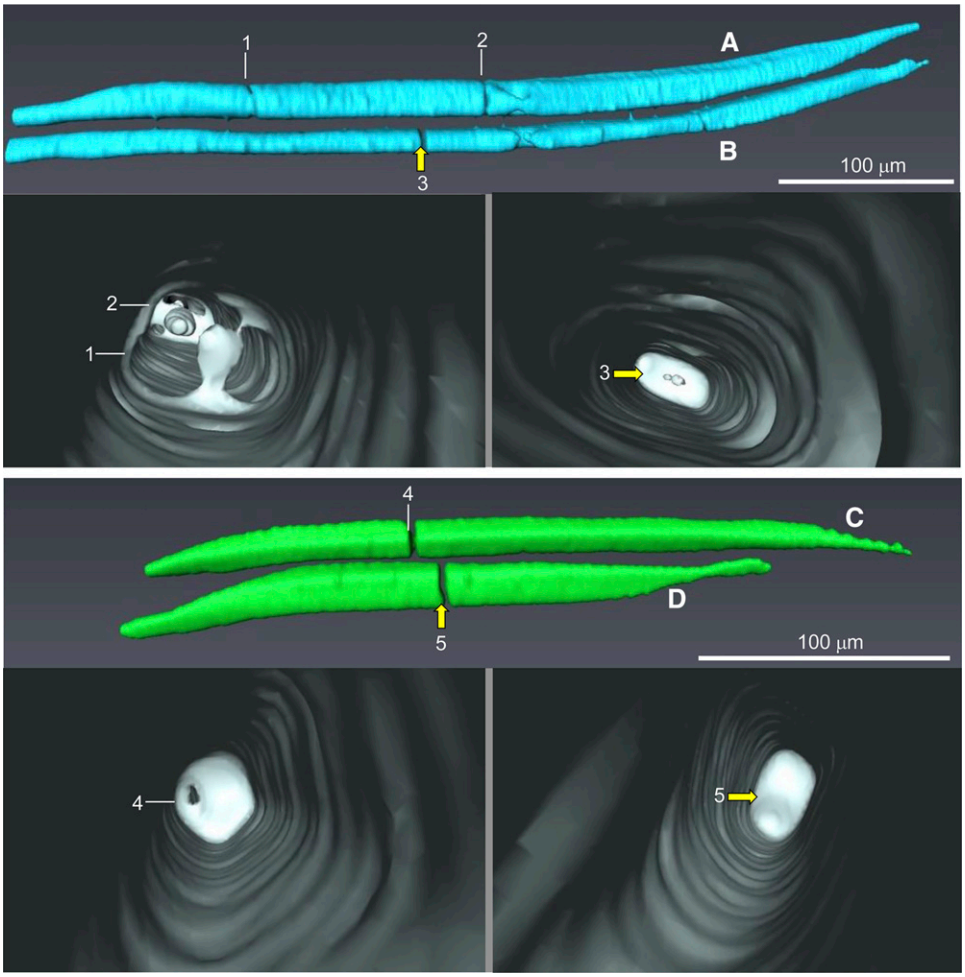

Figure 7. 3-D reconstructions of xylem vessel elements in the pedicel stem portion at 85 DAA (i.e. postveraison). Images were obtained from a dehydrated pedicel scanned at high resolution. At positions where vessel elements are constricted (A at positions 1 and 2 and C at position 4) or interrupted (B at position 3 and D at position 5), the deposition of some material is visualized inside the vessel lumen. Yellow arrows indicate the positions of blockages in the lumen of vessel elements.

For grape, several physiological parameters of the fruit (e.g. growth, sugar accumulation, turgor, and firmness) change before veraison (Thomas et al., 2008; Wada et al., 2008, 2009; Matthews et al., 2009), which is in line with the early developmental changes in pedicel k_h. The decrease in berry growth from stage I to stage II, which is a normal part of their development, may be directly related to the reduction in hydrostatic and osmotic pedicel k_h, which can reduce water transport capacity along the extracellular and intracellular pathways, respectively, between the parent plant and fruit. Developmental changes in fruit water relations, such as by a change of turgor of berry mesocarp cells and a drop in solute potential from stage I to III (Wada et al., 2008; Matthews et al., 2009), may aid water flow into the fruit when pedicel k_h declines.

Although reductions in the water transport capacity of grapevine stems (Brodersen et al., 2010, 2013) and petioles (Zufferey et al., 2011) are attributable to xylem embolisms, our microCT images provide direct evidence that in grape pedicels of well-watered vines, water transport capacity is not affected by air embolism formations, preveraison, and postveraison. Hydraulic measurements are in support of this observation, which show that both k_h values obtained under low and high ΔP declined in a similar fashion over fruit development. For example, if significant amounts of xylem embolisms had been present in the pedicel, then k_h as derived from high ΔP greater than 0.08 MPa should have remained constant over fruit development, because high pressures would flush embolized vessels. But this was not the case.

It could be argued that, during k_h measurements, ΔP applied initially was already too high and naturally occurring embolisms in the pedicel were already removed at the onset of the measurement. If this were true, the threshold value for a change of the pressure-flow relationship should be much less than 0.08 MPa. We tested this hypothesis by the application of an initial ΔP of less than 10 kPa (i.e. including native embolisms if present; Cochard et al., 2013) and subjected the pedicel to increasing ΔP steps of greater than 0.2 MPa (i.e. flushing embolisms) before returning to the initial ΔP and applying negative ΔP steps (Supplemental Fig. S2). We found that, in pedicels harvested both preveraison and postveraison, (1) the pressure threshold remained at 0.08 MPa, (2) the flow rate measured initially was similar to the one measured at a comparable ΔP following greater than 0.2 MPa, and (3) flow rates under $-\Delta P$ were similar to $+\Delta P$ of comparable absolute magnitude (i.e. negative pressure did not remove potential

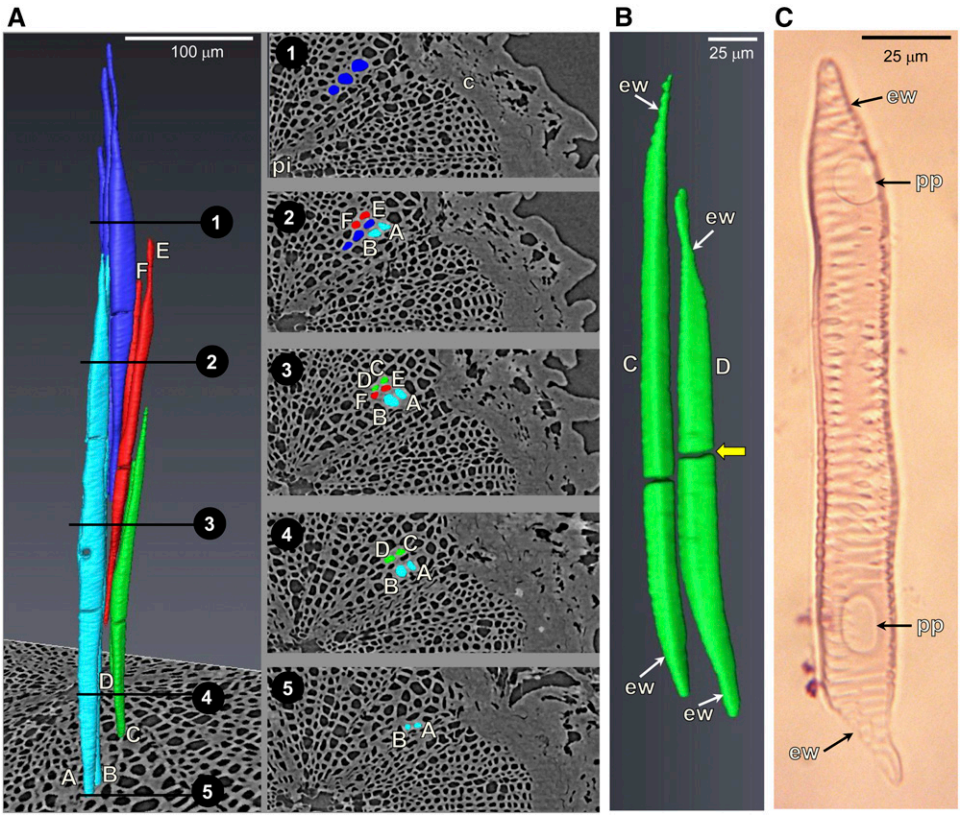

Figure 8. A, Structure and spatial arrangement of xylem vessel elements in the pedicel stem portion of a postveraison berry (85 DAA; vessels A–D are identical to Fig. 7). Vessel elements are not aligned vertically. For positions 1 to 5 along the pedicel, images on the right show the locations of vessel elements in 2-D projection. c, Cortex; pi, pith. B, Enlarged image of vessel elements C and D showing their tracheid-like structure with oblique end walls (ew). The yellow arrow indicates an interruption of vessel lumen. C, Pedicel vessel element extracted with the maceration technique showing oblique end walls and perforation plates (pp).

embolisms either). This proved the validity of the pressure-flow relationship and further supports that effects of xylem embolisms on pedicel k_h are negligible during the course of fruit development. Moreover, there is a possibility that embolized vessels in the pedicel may have refilled naturally during the time period of harvest and measurement, as has been reported for intact grapevines after 10 h (Brodersen et al., 2010), but this time period was less than 1 h when pedicel k_h was determined and, therefore, very unlikely. If grape pedicels possess the ability to repair xylem embolisms in a very short time period needs to be investigated in the future.

3-D microCT images provided clear evidence that losses in pedicel k_h between stage I and stage III were

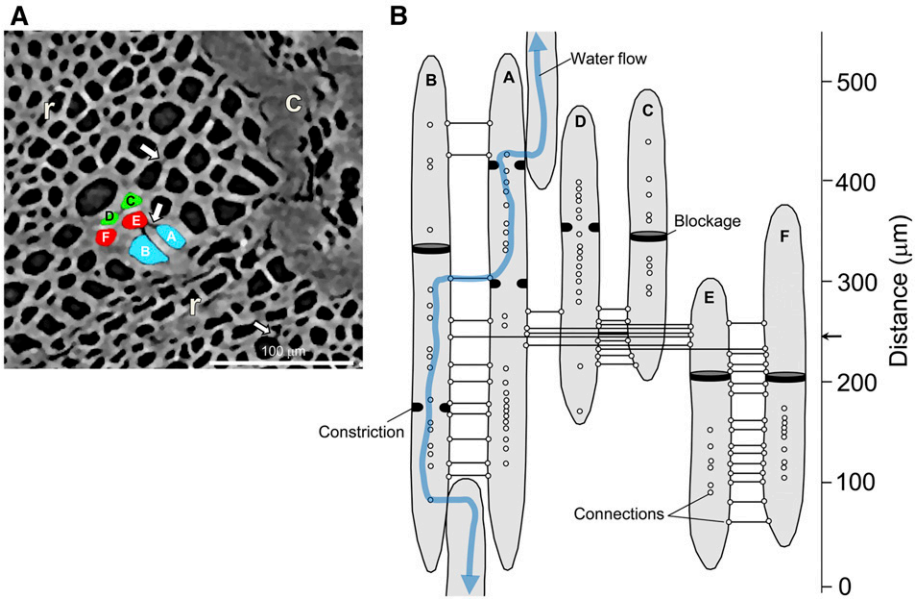

Figure 9. A, Examples of intervessel connections (white arrows) as detected in a transverse microCT image of the pedicel shown in Figure 8. c, Cortex; r, ray cells. B, Based on an analysis of the entire stack of transverse microCT images ($n > 1{,}000$), a map of intervessel connectivity was generated. Each circle represents the location of a connection along vessel elements. Solid lines indicate direct connections between vessel elements A to F. Positions of xylem blockages are indicated by black discs within the lumen of vessel elements. The blue line indicates a possible flow path of water through the pedicel even when some vessel elements are blocked locally.

associated with the formation of constrictions and ultimately blockages inside the lumen of xylem vessel elements (i.e. occlusions). Grapevine stems produce xylem blockages by tyloses (i.e. spherical shape) and gels in response to wounding (Sun et al., 2008). Even though Kasimatis (1957) thought that tyloses may exist in the pedicel postveraison, there is no direct evidence for tyloses in the berry (Chatelet et al., 2008a, 2008b) and the grape pedicel (Choat et al., 2009). Based on 3-D microCT images, xylem blockages in the pedicel exhibited irregular shapes, which suggest that they are not tyloses or remaining water menisci after dehydration and rather are composed of material such as polysaccharides (pectins and callose). The deposition of polysaccharide-like material in vessel elements of the pedicel might be associated with the developmental increase in sugar transport from the parent plant into the berry. Xylem blockages can explain the substantial reduction in pedicel k_h between stage I and stage III but might not solely explain the early developmental changes in pedicel k_h, because at 20 to 45 DAA, only approximately 6% of vessel elements were occluded (Table I). Those early changes may be related to additional functional and spatial changes of the pedicel xylem network (i.e. the clogging of interconnections between vessel elements; Fig. 9). It has been reported that intervessel pit resistance accounts for approximately 80% of the total hydraulic axial transport resistance in angiosperm trees (Choat et al., 2006), and variability in xylem hydraulic resistance has been associated with changes in vessel-to-vessel resistance (Zwieniecki et al., 2001). Due to the lack of relatively long and continuous vessels, it can be speculated that axial water movement through the pedicel strongly depends on the functional status of intervessel connections. Further work on the grape pedicel is needed to investigate (1) the exact timing of changes in pedicel k_h and xylem network functionality, (2) the chemical composition of material that blocks the lumen of vessel elements and potentially clogs intervessel pit connections, and (3) the mechanism involved in the formation of blockages with respect to the activity of living cells adjacent to vessel elements.

The importance of incorporating pedicel hydraulic properties in fruit growth models has been recognized by Hall et al. (2013), but the xylem tension (i.e. negative pressure) that manifests across the pedicel and, in turn, the water potential gradient ($\Delta\Psi$) is unknown (the tension is related to the water potential of plant and fruit that acts on both sides of the pedicel). For well-watered plants, as used here, we did not measure xylem tension directly, but we calculated that a $\Delta\Psi$ [$=Q \times (1/(k_h/\text{length}))$] of less than 5 kPa would be required across the pedicel to support xylem flows as measured in vivo between the parent plant and fruit by Greenspan et al. (1994; Supplemental Table S1). This is a small fraction of $\Delta\Psi$ of approximately 50 to 300 kPa, as measured between the parent plant and berry cluster (Greenspan et al., 1996). Whether a physical hydraulic barrier exists upstream of the pedicel (i.e. toward the rachis) that reduces the propagation of xylem tensions from the parent plant to the fruit remains unknown. In tomato, a fruit abscission zone is located in the knuckle midway along the pedicel with a large hydraulic resistance (Lee, 1989; Van Ieperen et al., 2003), and it may be that, for grape, a structure similar in its hydraulic property is located somewhere in the rachis. Hence, in the context of the intact plant, small tensions most likely exist across the pedicel xylem, at least under well-watered conditions, which may explain the negligible amounts of xylem embolisms. However, it needs to be shown if embolism formation in the pedicel remains negligible also under drought conditions and if the hydraulic architecture of the pedicel is an adaptation to minimize embolism susceptibility.

It has been proposed that the maintenance of a partially functional xylem path is important to recycle excess water that enters the fruit via the phloem during ripening (Greenspan et al., 1994; Garcia-Luis et al., 2002; Keller et al., 2006). Postveraison, the amount of daily xylem backflow in grape was estimated to be

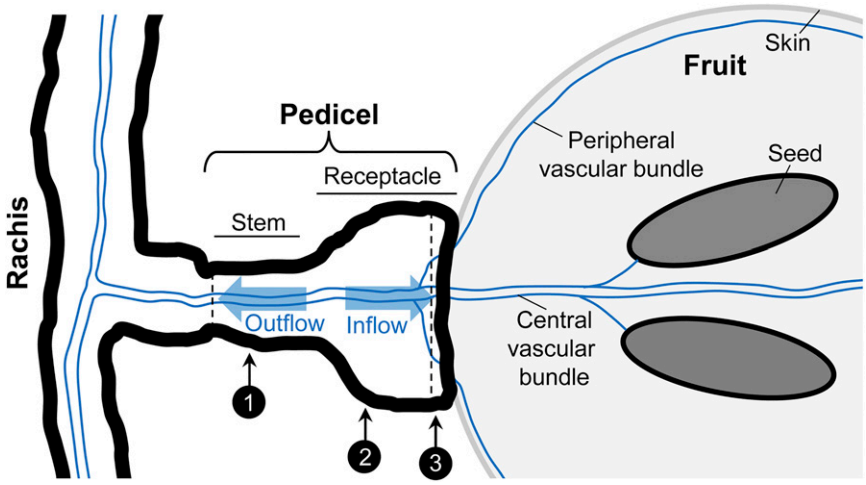

Figure 10. Schematic drawing of rachis, pedicel, and fruit in grapevine. The vascular system (blue lines) of fruit and rachis via the pedicel is illustrated. The pedicel is composed of a narrower stem portion and wider receptacle portion. In this study, pedicel anatomy and xylem function were analyzed at up to three positions along the pedicel, as indicated by numbers. Hydraulic properties were measured on excised pedicels (dashed lines indicate the positions of cuts) using a modified pressure-probe system.

approximately 33% of fruit volume, a relatively high level (Choat et al., 2009). Our microCT data highlight that xylem vessel elements in the pedicel are interconnected postveraison, which most likely secures a xylem flow path even in the presence of xylem blockages. Based on the observations of Choat et al. (2009), intervessel connection as detected here are most likely bordered pits. Moreover, we can exclude that a rectification of xylem flow resides in the grape pedicel and contributes to the changing water flow dynamics between the parent plant and fruit over development, as suggested by Tilbrook and Tyerman (2009), because inflow k_h was similar to outflow k_h.

CONCLUSION

Grape pedicel k_h declines before veraison and gradually over fruit development, which is associated with the formation of blockages in the lumen of vessel elements. However, due to the fact that, postveraison, approximately 50% of vessel elements in the pedicel stem portion remained functional and were not occluded and vessel elements were interconnected, our data suggest that a functional xylem flow pathway of reduced k_h still exists late into berry ripening. These findings provide a basis for further anatomical, physiological, and molecular research into the role of the grape pedicel in affecting berry growth and development.

MATERIALS AND METHODS

Plant Material

Own-rooted grapevines (*Vitis vinifera* 'Cabernet Sauvignon') were grown in a greenhouse (temperature of 20°C–30°C, relative humidity of 40%–70%, and natural light with a daily maximum of 1,200 μmol photons m^{-2} s^{-1} photosynthetically active radiation) at the University of California (Davis). Vines were about 2 years old and maintained in 2-gallon plastic pots (depth approximately 46 cm, width approximately 20 cm) filled with a soil mix of one-third peat, one-third sand, and one-third redwood compost. In total, 15 plants were used for experiments. Each plant had two to three shoots that were vertically trained to approximately 1.5 m (n = 3–4 berry clusters per shoot, more than 100 berries per cluster). Pots were drip irrigated three times per day with water supplemented with calcium (90 μg mL^{-1}), magnesium (24 μg mL^{-1}), potassium (124 μg mL^{-1}), nitrogen as NH_4^+ (6 μg mL^{-1}), nitrogen as NO_3^- (96 μg mL^{-1}), phosphorus (26 μg mL^{-1}), sulfur (16 μg mL^{-1}), iron (1.6 μg mL^{-1}), manganese (0.27 μg mL^{-1}), copper (0.16 μg mL^{-1}), zinc (0.12 μg mL^{-1}), boron (0.26 μg mL^{-1}), and molybdenum (0.016 μg mL^{-1}) at pH 5.5 to 6. Berry clusters were tagged when 50% of the cluster was flowering (i.e. day of anthesis).

Hydraulic Measurements

In the greenhouse, two to three fruits located midway along the berry cluster were cut off under water with scissors from the rachis, placed in a moist plastic container, and transported within 30 min to the laboratory. In the laboratory, the pedicel end was recut under water with a fresh razor blade, and subsequently, the pedicel was excised from the fruit at the receptacle end (Fig. 10). Pedicel diameter and length, as well as fruit diameter, were measured with an electronic hand-held caliper (Y513446; Fisher Scientific). The solute potential of berry sap was measured using osmometry (5500 vapor pressure osmometer; Wescor). Hydraulic properties of excised pedicels were measured using a modified pressure-probe system together with a computer-vision-based meniscus tracker (Wong et al., 2009; Supplemental Fig. S1). Typically a reliable measure of pedicel hydraulic property was obtained for one out of three pedicels from the same berry cluster, and pedicels measured at different DAA were sampled randomly from different vines and berry clusters.

For hydrostatic experiments, approximately 2 mm of the pedicel stem portion was inserted into a 10-mm-long adapter piece that was attached to a glass microcapillary (0.75-mm i.d.; Stoelting). The pedicel stem portion was sealed with superglue (Loctite gel; Henkel). The microcapillary was half-filled with deionized water (diH_2O) and backfilled with silicone oil (dimethyl silicone fluid; Thomas Scientific), which created an oil-water meniscus. The microcapillary was connected to the probe via a compression seal, and the pedicel receptacle was submerged into a diH_2O bathing solution. Hydrostatic water flows across the pedicel were induced by the application of multiple step changes in hydrostatic pressure (−0.05 to 0.22 MPa), while each hydrostatic pressure step was clamped for about 5 to 15 s; step changes of increasing and decreasing hydrostatic pressure applied for the same pedicel showed that water flow rates were reversible. During each hydrostatic pressure step, the displacement of the meniscus (d) was followed with a digital camera, recorded every 0.133 s, and changes in volume (V) were derived from changes in displacement [i.e. $V = 3.14 \times (\text{radius of capillary})^2 \times d$]. The Q under each applied pressure gradient across the pedicel was determined from the slope of the linear regression line of volume versus time. Positive applied pressure induced water flow from the pedicel stem to the receptacle end (inflow), and negative applied pressure induced water flow in the reverse direction (outflow or backflow). When water leaked through any connections of pedicel and microcapillary, or air bubbles were present in the microcapillary, measurements were discarded.

For osmotic experiments, the excised pedicel segment was fixed to the glass microcapillary as described for hydrostatic experiments; the microcapillary was half-filled with diH_2O, and the pedicel receptacle end was bathed in different Suc concentrations with osmotic pressures of 0.63, 1.88, and 3.13 MPa. Osmotic pressures of Suc solutions were in the range of osmotic pressure of extracted fruit sap. Each Suc solution (i.e. osmotic pressure step) was applied for 10 to 15 min before being exchanged to another one of higher concentration, and finally, the Suc solution of lowest concentration was applied again to check for reversibility in flow. Due to the much longer time required to accurately measure volume in osmotic (approximately 15 min) as compared with hydrostatic (less than 15 s) experiments, only one osmotic pressure step was applied twice. During each osmotic pressure step, the displacement of the air/water meniscus was followed with the digital camera, and Q was determined as described for hydrostatic experiments.

Hydraulic properties of the pedicel were defined according to the terminology of Tyree and Ewers (1991). From both hydrostatic and osmotic experiments, pedicel k_h was determined from the slope (m) of the linear part of the pressure-flow relationship and normalized for pedicel length (l) according to $k_h = [m \times l]$. In hydrostatic experiments, the relationship of ΔP versus Q was typically linear for ΔP of 0.08 MPa or less and ΔP of more than 0.08 MPa (Fig. 3A); subsequently, k_h was determined separately for both low- and high-pressure ranges. When for ΔP greater than 0.08 MPa a reliable Q was obtained only from a single ΔP, due to problems of water leakage at higher applied pressures, k_h was determined by $[(Q/\Delta P)l]$. Pedicel hydrostatic k_h under inflow and outflow conditions was determined from slope values corresponding to ΔP of −0.05 to 0 MPa and ΔP of 0 to 0.0.8 MPa, respectively.

Pedicel k_s was determined by normalizing hydrostatic k_h as measured under low ΔP of −0.05 to 0.08 MPa for the A_x of either the pedicel stem or receptacle portion according to $k_s = [k_h/A_x]$. To obtain k_s for each pedicel, A_x was derived from diameter measurements of pedicel stem [$A_x = 0.159 \times (\text{diameter}/2)^2 \times 3.14$; $r^2 = 0.91$, $P < 0.0001$] and receptacle [$A_x = 0.0866 \times (\text{diameter}/2)^2 \times 3.14$; $r^2 = 0.83$, $P < 0.0001$] portions after hydraulic analysis. For both pedicel portions, the relationship of A_x versus diameter was established by measuring A_x from free-hand cross sections (as described below) and corresponding pedicel diameters (n = 28 pedicels analyzed between 20 and 90 DAA).

Light Microscopy

Free-hand cross sections were made with a fresh razor blade at three different positions along the pedicel (Fig. 10). Unstained sections were mounted on a slide in diH_2O and observed under violet fluorescent light (excitation filter, 400- to 410-nm peak emission; dichromatic mirror, 455 nm; and barrier filter, 455 nm) with an Olympus Vanox-AHBT (Olympus America) compound microscope connected to a 600ES digital camera (Pixera). Lignified tissue emitted a bright blue autofluorescence signal. Images were analyzed using Fiji image software (www.fiji.sc; ImageJ), A_x was determined using the Polygon selection tool, and the number and diameter of xylem elements were determined using the Analyze particle tool (Supplemental Fig. S3).

Maceration was used as described by Chatelet et al. (2008b) to investigate vessel anatomical structure. Briefly, cross sections approximately 2 mm thick of a preveraison pedicel were immersed in maceration solution (30% [v/v] hydrogen peroxide, acetic acid, and distilled water), placed in an oven at 57°C for up to 24 h, subsequently shaken to loosen tissue, stained with Safranin O that strongly binds to lignin, and finally, the solution was pipetted onto a slide and viewed with the Olympus Vanox-AHBT compound microscope.

microCT

Pedicels were imaged at the x-ray microtomography facility at the Lawrence Berkeley National Laboratory Advanced Light Source (Beamline 8.3.2). To determine whether embolized xylem conduits existed in the pedicel, entire berry clusters were cut off with scissors under water at the rachis, placed in a moist aluminum-covered plastic bag, and transported by car from the University of California to the Advanced Light Source. Within 20 h after harvest, a pedicel was extracted under water with a fresh razor blade from fruit and rachis, as described for hydraulic measurements, fixed on a solid stage at the receptacle end with adhesive putty, and rotated in the 17- to 19-keV synchrotron x-ray beam in 0.176° increments over 180°, yielding 1,025 2-D projection images with a 1.78-μm voxel resolution captured on a scientific complementary metal-oxide semiconductor camera (PCE.edge [PCO AG]; Brodersen et al., 2010, 2013). For a more detailed analysis of vessel structure and spatial arrangement, excised pedicels were dehydrated for 24 h (Figs. 7–9) and 4 d (Fig. 6) at approximately 30°C prior to scanning. For imaging, the receptacle end was fixed with epoxy glue (20445 Flow-Mix 5-Minute Epoxy; Devcon) to a 2-cm-long metal rod (2-mm diameter), which was inserted into a rotating drill chuck. This minimized vibrations and lateral pedicel movements during scanning. Dehydrated pedicels were imaged in the stem portion at either 1.78- or 0.89-μm voxel resolution. We focused on the pedicel stem and not the receptacle portion because, along the length of the stem portion, the arrangement of the xylem vessel was most uniform. After a scan was completed, the acquired 2-D projection images were reconstructed into a stack of transverse images using a custom software plugin for Fiji image-processing software (www.fiji.sc; ImageJ) that used Octopus 8.3 software (Institute for Nuclear Sciences, Ghent University) in the background. After uploading the entire stack of TIF images into AVIZO 6.2 software (VSG), 3-D images were generated of the pedicel surface using the Volume rendering module and of xylem vessel elements using the Label-field segmentation editor and SurfaceGen volume rendering module. In order to determine the frequency of vessel elements with blockages (i.e. occlusion) in the pedicel, a transverse image slice within the stack of 2-D images of the pedicel stem portion was selected, and 40 to 60 vessel elements intersecting this slice were generated in 3-D images (as described above). Generated vessel elements that provided sufficient spatial and visual resolution were included in this analysis, and the lumen of vessel elements was evaluated for the presence of blockages along their entire axial distance.

Data Analysis

Data were analyzed using SAS (version 9.2; SAS Institute) and SigmaPlot (version 8.0, Systat Software). For linear regression analyses, the PROC REG procedure was used. For fitting of smoothed trend lines, the PROC TRANSREG procedure was used. Average values and SD were determined using the PROC MEANS procedure. For statistical analysis, data were subjected to the PROC GLM procedure followed by the Tukey-Kramer test using SAS or Student's *t* test using SigmaPlot.

Supplemental Data

The following supplemental materials are available.

Supplemental Figure S1. Schematic presentation of the modified pressure-probe system used to measure pedicel hydraulic properties.

Supplemental Figure S2. Image of the pedicel stem portion showing lignified xylem tissue excluding ray cells and diameter distribution of xylem elements.

Supplemental Figure S3. Pedicel hydraulic characteristics in response to a series of applied pressure steps as measured with a bellows pressure probe.

Supplemental Table S1. Estimation of the $\Delta\Psi$ across the pedicel.

ACKNOWLEDGMENTS

We thank David Chatelet (Brown University) for providing the image of the macerated xylem vessel, Judy Jernstedt (University of California, Davis) for help with anatomy, Ca-Western Nurseries (Visalia, CA) for donating the grapevines, and Dula Parkinson and Alastair MacDowell for assistance at the Lawrence Berkeley National Laboratory Advanced Light Source Beamline 8.3.2 microtomography facility.

Received January 10, 2015; accepted June 12, 2015; published June 15, 2015.

LITERATURE CITED

Bondada BR, Matthews MA, Shackel KA (2005) Functional xylem in the post-veraison grape berry. J Exp Bot **56:** 2949–2957

Brodersen CR, McElrone AJ, Choat B, Lee EF, Shackel KA, Matthews MA (2013) In vivo visualizations of drought-induced embolism spread in *Vitis vinifera*. Plant Physiol **161:** 1820–1829

Brodersen CR, McElrone AJ, Choat B, Matthews MA, Shackel KA (2010) The dynamics of embolism repair in xylem: in vivo visualizations using high-resolution computed tomography. Plant Physiol **154:** 1088–1095

Chatelet DS, Rost TL, Matthews MA, Shackel KA (2008a) The peripheral xylem of grapevine (*Vitis vinifera*) berries. 2. Anatomy and development. J Exp Bot **59:** 1997–2007

Chatelet DS, Rost TL, Shackel KA, Matthews MA (2008b) The peripheral xylem of grapevine (*Vitis vinifera*). 1. Structural integrity in post-veraison berries. J Exp Bot **59:** 1987–1996

Choat B, Brodie TW, Cobb AR, Zwieniecki MA, Holbrook NM (2006) Direct measurements of intervessel pit membrane hydraulic resistance in two angiosperm tree species. Am J Bot **93:** 993–1000

Choat B, Gambetta GA, Shackel KA, Matthews MA (2009) Vascular function in grape berries across development and its relevance to apparent hydraulic isolation. Plant Physiol **151:** 1677–1687

Cochard H, Badel E, Herbette S, Delzon S, Choat B, Jansen S (2013) Methods for measuring plant vulnerability to cavitation: a critical review. J Exp Bot **64:** 4779–4791

Coombe BG, McCarthy MG (2000) Dynamics of grape berry growth and physiology of ripening. Aust J Grape Wine Res **6:** 131–135

Fouquet R, Léon C, Ollat N, Barrieu F (2008) Identification of grapevine aquaporins and expression analysis in developing berries. Plant Cell Rep **27:** 1541–1550

Garcia-Luis A, Oliveira ME, Bordon Y, Siqueira DL, Tominaga S, Guardiola JL (2002) Dry matter accumulation in citrus fruit is not limited by transport capacity of the pedicel. Ann Bot (Lond) **90:** 755–764

Greenspan MD, Schultz HR, Matthews MA (1996) Field evaluation of water transport in grape berries during water deficits. Physiol Plant **97:** 55–62

Greenspan MD, Shackel KA, Matthews MA (1994) Developmental changes in the diurnal water budget of the grape berry exposed to water deficits. Plant Cell Environ **17:** 811–820

Hall AJ, Minchin PE, Clearwater MJ, Génard M (2013) A biophysical model of kiwifruit (*Actinidia deliciosa*) berry development. J Exp Bot **64:** 5473–5483

Hall GE, Bondada BR, Keller M (2011) Loss of rachis cell viability is associated with ripening disorders in grapes. J Exp Bot **62:** 1145–1153

Horbens M, Feldner A, Höfer M, Neinhuis C (2014) Ontogenetic tissue modification in *Malus* fruit peduncles: the role of sclereids. Ann Bot (Lond) **113:** 105–118

Kasimatis AN (1957) Some factors influencing the development of water berries in Thompson Seedless grapes grown for table use. PhD thesis. University of California, Davis

Keller M, Smith JP, Bondada BR (2006) Ripening grape berries remain hydraulically connected to the shoot. J Exp Bot **57:** 2577–2587

Krasnow M, Matthews M, Shackel K (2008) Evidence for substantial maintenance of membrane integrity and cell viability in normally developing grape (*Vitis vinifera* L.) berries throughout development. J Exp Bot **59:** 849–859

Lang A, Ryan KG (1994) Vascular development and sap flow in apple pedicels. Ann Bot (Lond) **74:** 381–388

Lee DR (1989) Vasculature of the abscission zone of tomato fruit: implications for transport. Can J Bot **67:** 1898–1902

Malone M, Andrews J (2001) The distribution of xylem hydraulic resistance in the fruiting truss of tomato. Plant Cell Environ **24:** 565–570

Matthews MA, Shackel KA (2005) Growth and water transport in fleshy fruit. *In* NM Holbrook, MA Zwieniecki, eds, Vascular Transport in Plants. Elsevier Academic Press, Burlington, VT, pp 181–197

Matthews MA, Thomas TR, Shackel KA (2009) Fruit ripening in *Vitis vinifera* L.: possible relation of veraison to turgor and berry softening. Aust J Grape Wine Res **15:** 278–283

Mazzeo M, Dichio B, Clearwater MJ, Montanaro G, Xiloyannis C (2013) Hydraulic resistance of developing *Actinidia* fruit. Ann Bot (Lond) **112:** 197–205

Nii N, Coombe BG (1983) Structure and development of the berry and pedicel of the grape *Vitis vinifera* L. Acta Hortic **139:** 129–140

Rancić D, Quarrie SP, Radosević R, Terzić M, Pećinar I, Stikić R, Jansen S (2010) The application of various anatomical techniques for studying the hydraulic network in tomato fruit pedicels. Protoplasma **246:** 25–31

Rancić D, Quarrie SP, Terzić M, Savić S, Stikić R (2008) Comparison of light and fluorescence microscopy for xylem analysis in tomato pedicels during fruit development. J Microsc **232:** 618–622

Rogiers SY, Smith JA, White R, Keller M, Holzapfel BP, Virgona JM (2001) Vascular function in berries of *Vitis vinifera* (L) cv. Shiraz. Aust J Grape Wine Res **7:** 47–51

Steudle E (2000) Water uptake by roots: effects of water deficit. J Exp Bot **51:** 1531–1542

Sun Q, Rost TL, Matthews MA (2008) Wound-induced vascular occlusions in Vitis vinifera (Vitaceae): tyloses in summer and gels in winter. Am J Bot **95:** 1498–1505

Thomas TR, Shackel KA, Matthews MA (2008) Mesocarp cell turgor in *Vitis vinifera* L. berries throughout development and its relation to firmness, growth, and the onset of ripening. Planta **228:** 1067–1076

Tilbrook J, Tyerman SD (2009) Hydraulic connection of grape berries to the vine: varietal differences in water conductance into and out of berries, and potential for backflow. Funct Plant Biol **36:** 541–550

Tyerman SD, Tilbrook J, Pardo C, Kotula L, Sullivan W, Steudle E (2004) Direct measurement of hydraulic properties in developing berries of *Vitis vinifera* L. cv Shiraz and Chardonnay. Aust J Grape Wine Res **10:** 170–181

Tyree MT, Ewers FW (1991) The hydraulic architecture of trees and other woody plants. New Phytol **119:** 345–360

Van Ieperen W, Volkov VS, Van Meeteren U (2003) Distribution of xylem hydraulic resistance in fruiting truss of tomato influenced by water stress. J Exp Bot **54:** 317–324

Wada H, Matthews MA, Shackel KA (2009) Seasonal pattern of apoplastic solute accumulation and loss of cell turgor during ripening of *Vitis vinifera* fruit under field conditions. J Exp Bot **60:** 1773–1781

Wada H, Shackel KA, Matthews MA (2008) Fruit ripening in Vitis vinifera: apoplastic solute accumulation accounts for pre-veraison turgor loss in berries. Planta **227:** 1351–1361

Wong ES, Slaughter DC, Wada H, Matthews MA, Shackel KA (2009) Computer vision system for automated cell pressure probe operation. Biosystems Eng **103:** 129–136

Zufferey V, Cochard H, Ameglio T, Spring JL, Viret O (2011) Diurnal cycles of embolism formation and repair in petioles of grapevine (*Vitis vinifera* cv. Chasselas). J Exp Bot **62:** 3885–3894

Zwieniecki MA, Melcher PJ, Holbrook NM (2001) Hydrogel control of xylem hydraulic resistance in plants. Science **291:** 1059–1062